© 2022. Published by The Company of Biologists Ltd | Journal of Experimental Biology (2022) 225, jeb244079. doi:10.1242/jeb.244079

METHODS & TECHNIQUES

A brainstem preparation allowing simultaneous access to respiratory motor output and cellular properties of motoneurons in American bullfrogs

Lara do Amaral-Silva* and Joseph M. Santin*

ABSTRACT

Breathing is generated by a complex neural circuit, and the ability to monitor the activity of multiple network components simultaneously is required to uncover the cellular basis of breathing. In neonatal rodents, a single brainstem slice can be obtained to record respiratory-related motor nerve discharge along with individual rhythm-generating cells or motoneurons because of the close proximity of these neurons in the brainstem. However, most *ex vivo* preparations in other vertebrates can only capture respiratory motor outflow or electrophysiological properties of putative respiratory neurons in slices without relevant synaptic inputs. Here, we detail a method to horizontally slice away the dorsal portion of the brainstem to expose fluorescently labeled motoneurons for patch-clamp recordings in American bullfrogs. This 'semi-intact' preparation allows tandem recordings of motor output and single motoneurons during respiratory-related synaptic inputs. The rhythmic motor patterns are comparable to those from intact preparations and operate at physiological temperature and [K^+]. Thus, this preparation provides the ability to record network and cellular outputs simultaneously and may lead to new mechanistic insights into breathing control across vertebrates.

KEY WORDS: Breathing control, Frogs, *In vitro* preparation, Motoneurons, Patch-clamp, Respiratory-related synaptic inputs

INTRODUCTION

Ventilation is generated by a brainstem neural circuit that includes rhythm-generating, chemosensory, modulatory areas and motoneurons. Understanding how these elements come together to control breathing is critical not only to study prevalent health issues associated with disordered ventilation but also for answering major questions in vertebrate physiology. Among the approaches used to analyze these circuits in vertebrates, *in vitro* preparations stand out for allowing a direct and detailed study of neural respiratory function. In this case, intact brainstem and brain slice preparations are most often used. Fictive respiratory motor output from the intact brainstem can be recorded from nerve roots that innervate muscles involved in breathing to answer questions regarding rhythm generation, chemosensation and plasticity (Burton and Santin, 2020; Johnson et al., 2007; Smith and Feldman, 1987; Vincen-Brown et al., 2016; Wilson et al., 2000). However, in this preparation, only the motor output of a complex respiratory network is assessed, providing no cell level information. In contrast, recording from respiratory-related neurons in brain slices allows detailed analysis of cellular physiology but necessarily cuts away relevant synaptic connections from the network needed to understand how they function physiologically (Bueschke et al., 2021a; Janes et al., 2019a; Lape and Nistri, 2000; Santin et al., 2017). As an exception, a ∼600-µm-thick brainstem slice of neonatal rodents can encompass rhythm generator, modulatory regions, hypoglossal motoneurons and the hypoglossal motor root because of their close proximity in the slice (Funk and Greer, 2013). Combining network-level and cellular physiology investigations has been more difficult in adult rats and other air-breathing vertebrates that have respiratory regions more diffusely spread throughout the brainstem.

Anuran amphibians have provided important comparative insights into the function of the respiratory network. As these animals breathe water as tadpoles and air as adults, they make unique models to understand the neural basis for the development and evolution of air breathing (Burggren and Infantino, 1994; Janes et al., 2019b; Perry et al., 2001). In this way, amphibians have held the interest of respiratory neurobiologists for decades, with recent advancements in the function of respiratory motoneurons for the development of air breathing, respiratory pattern formation and breathing modulation (Bueschke et al., 2021a; Fonseca et al., 2021; Gargaglioni and Milsom, 2007; Hedrick, 2005; Janes et al., 2019a; Kogo and Remmers, 1994; Kottick et al., 2013; West and Jones, 1975; Wilson et al., 2002). Moreover, some anurans present a wide range of tolerance to harsh environmental conditions such as hypoxia/ischemia, hypercapnia and temperature (Bueschke et al., 2021b; Reid, 2006; Santin and Hartzler, 2016), providing insights into the robustness of nervous system function to environmental stressors. Despite historical and growing interest in the amphibian respiratory network, little is known about the cellular and synaptic mechanisms of respiratory motor function as only the output of the entire network or isolated cells in slices is commonly studied separately. Thus, a new preparation had to be designed to investigate cellular physiology together with network activity. Addressing this demand, we developed an *in vitro* preparation that maintains the network intact while exposing motoneurons for whole-cell current and voltage-clamp recordings during the ongoing respiratory rhythm.

MATERIALS AND METHODS

Animals

All experimental procedures received prior approval from the Institutional Animal Care and Use Committee at The University of North Carolina at Greensboro (protocol 19-006). Experiments were performed in 10 adult female American bullfrogs, *Lithobates*

Department of Biology, University of North Carolina at Greensboro, Greensboro, NC 27403, USA.

*Authors for correspondence (l_doamarals@uncg.edu, jmsantin@uncg.edu)

L.d.A.-S., 0000-0001-6273-3240; J.M.S., 0000-0003-1308-623X

Received 29 January 2022; Accepted 6 May 2022

Journal of Experimental Biology (2022) 225, jeb244079. doi:10.1242/jeb.244079

catesbeianus (Shaw 1802), weighing 100±15 g acquired from Rana Ranch (Twin Falls, ID, USA). Upon arrival, frogs were maintained in plastic tanks containing aerated and dechlorinated tap water and a dry area. Pelleted food from Rana Ranch was provided to the frogs once a week. The tanks were kept at room temperature within a range of 22–25°C and a 12 h:12 h light:dark cycle. All animals were acclimated to the lab for at least a week prior to the experiments. Although only females were used in this study, we do not expect any morphological difference in the brainstem of males that would impact the development of the preparation described below.

Dissection

The animals were deeply anesthetized using ∼1 ml of isoflurane in a 1 liter sealed container, as verified by loss of the toe-pinch reflex. This was followed by decapitation. Immediately, the head was immersed in 4°C artificial cerebrospinal fluid (aCSF, in mmol l^{-1}: 104 NaCl, 4 KCl, 1.4 $MgCl_2$, 7.5, D-glucose, 40 $NaHCO_3$, 2.5 $CaCl_2$ and 1 NaH_2PO_4) gassed with 1.5% CO_2 and 98.5% O_2 (pH 7.85), and decerebration was quickly performed. The skull and bones covering the brainstem were removed, and the brainstem–spinal cord was carefully excised from the skull as previously described (Adams et al., 2021; Burton and Santin, 2020). The dura membrane covering the brainstem–spinal cord was then excised, and the preparation was transected rostrally at the diencephalon and the caudal side immediately rostral to the brachial plexus (Fig. 1A).

Motoneuron labeling

The brainstem–spinal cord was pinned ventral side up in a 6 ml Sylgard-coated (184, Dow Chemicals, Midland, MI, USA) Petri dish. Room temperature (22±1°C) aCSF bubbled with 1.5% CO_2 and 98.5% O_2 was circulated in the dish using a peristaltic pump at ∼7 ml min^{-1} (Mini Pump Variable Flow, Fisher Scientific, Hampton, NH, USA). The fourth branch of the vagal nerve (cranial nerve X; CNX) was isolated in order to label laryngeal branch motoneurons that innervate the glottal dilator, a respiratory muscle in anuran amphibians (Kogo and Remmers, 1994; Kogo et al., 1994; Sakakibara, 1984). Vagus cell bodies were labeled by backfilling the nerve using a dextran tetramethylrhodamine 3000 MW lysine fixable dye (Invitrogen – Thermo Fisher, Waltham, MA, USA). To do so, the root was pulled into a fire-polished glass pipette made to fit tight around the nerve and approximately 1 µl of 10% dextran was loaded into the tip of the glass pipette. Both vagal roots were backfilled; the first side was loaded for 1 h, and immediately the opposite side was loaded for 2 h (Fig. 1A). This produced robustly labeled neurons for electrophysiological recording as previously described in bullfrog brainstem slices (Burton and Santin, 2020; Santin et al., 2017; Zubov et al., 2021, 2022 preprint).

Slicing

Extracellular nerve recordings (details below) were acquired from all intact brainstem–spinal cord preparations before slicing to compare activity with the semi-intact preparation after slicing. To slice only the caudal part of the brainstem, we first cut a block of 5% agar (Difco Laboratories, Plymouth, MI, USA) of 9±0.5 mm height, 8 mm width and 12.5 mm length, and one half was cross-sectioned at a 45 deg angle (Fig. 1B). Low electroendosmosis agarose (Sigma-Aldrich, St Louis, MO, USA) was prepared at a 2% concentration in 1% PBS (Gibco – Thermo Fisher) using a heating and stirring plate. Once the boiling point was achieved, the agarose beaker was transferred to a heating plate set at 50°C, and the agarose temperature was measured with a digital thermometer (Extech Instruments 421504, Nashua, NH, USA). Once the agarose had cooled to 45°C, the surface of the agar block was briefly heated using a flat piece of metal that had been heated using an alcohol burner, so a fine layer of agarose poured with a disposable pipette could adhere to it. Immediately after that, the brain was positioned on the agar block with the rostral part at a 45 deg angle. The vagal root was used as a landmark that should be over the angled edge (between 45 and 0 deg), maintaining the caudal part of the brainstem–spinal cord over the horizontal site of the block (Fig. 1B). The caudal site of the spinal cord was pinned to ensure it stayed in place and a drop of agarose was quickly poured over the caudal site covering all the area at 0 deg angle. The stabilization of the preparation using agarose is a critical step for slicing. It was designed after several unsuccessful attempts to stabilize the preparation using pins, which does not provide enough stability for precise slicing, or different types of glue, which adhere permanently to the preparation, often gluing the nerve roots (rendering it unusable) and preventing adequate oxygenation. After the agarose step, the block with the embedded brain was glued on the vibratome plate (Technical Products International series 1000, St Louis, MO, USA) using super glue. The preparation was immediately covered in oxygenated cold aCSF solution (4°C), and the pin holding the caudal site was removed. In sequence, 200 µm slices with amplitude 7 were taken from the dorsal surface of the preparation until we approached the bottom of the 4th ventricle in the region between the vagal (X) and hypoglossal (H) nerves. After that, the preparation was finely sliced (10–50 µm) until the vagal cell region was exposed (see Fig. 1B). The slicing proportions utilized here aimed to have most of the vagal motoneurons exposed for patch-clamp analysis and also to protect the lung generator area from being sliced. This is also essential for the success of the semi-intact preparation as we observed that the respiratory rhythm was particularly disrupted when slicing over the lung rhythm generator area. Because the vagal motor pool is spread longitudinally and the most rostral area is closer to the lung rhythm generator (Baghdadwala et al., 2015; Matesz and Székely, 1996; Vasilakos et al., 2005), the preparation had a caudal bias. The most rostral part of the vagal nuclei was over the 45 deg angle during slicing and, thus, cells in this area were usually deeper in the tissue unavailable for patch-clamp recording.

A chamber for electrophysiology recordings (RC26G, Warner Instruments, Holliston, MA, USA) was previously adhered to a coverslip using silicon and the recording part was coated with a thin layer of Sylgard. The semi-intact preparation was pinned in this chamber using Teflon-coated wire (size 003, Medwire Corp, Mt Vernon, NY, USA). Two pins were placed above the tectum, two in the extreme lateral region of the cerebellum, two in the lateral region between the vagal and hypoglossal nerves, and finally three on the most caudal site of the preparation (Fig. 1C). The pinned semi-intact preparation was left to recover in the chamber, circulated with oxygenated aCSF for an hour before recordings.

Extracellular and electrophysiological recordings

The chamber containing the semi-intact preparation was placed under a fixed-stage microscope (FN1, Nikon Instruments Inc., Melville, NY, USA) coupled to a real-time imaging camera (Hamamatsu ORCA Flash 4.0LT sCMOS, Hamamatsu Photonics, Hamamatsu City, Japan). The preparation was continuously superfused with aCSF gassed with 1.5% CO_2 and 98.5% O_2 by a

Journal of Experimental Biology (2022) 225, jeb244079. doi:10.1242/jeb.244079

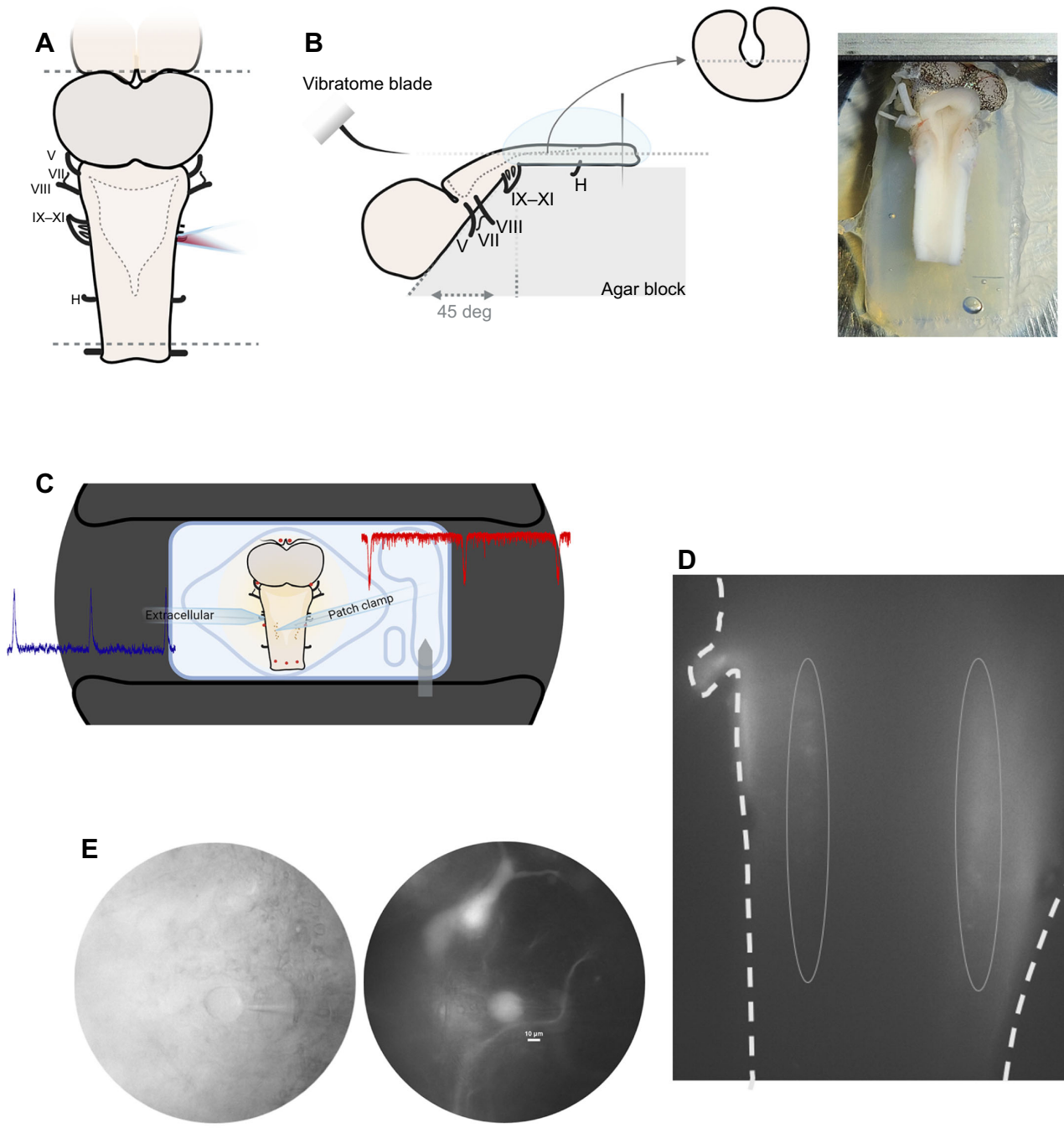

Fig. 1. Procedures to record vagal motoneurons and rootlet simultaneously. (A) Schematic diagram of the dissected brainstem showing dye loading on the vagal root (CNX). (B) Brainstem prepared for slicing. Left: diagram showing the brainstem adhered to agar by agarose with the vagal root at the 0 to 45 deg transition. The vibratome blade slices the dorsal part of the brainstem covered by agarose until the bottom of the 4th ventricle is reached in the region between the vagal (X) and hypoglossal (H) nerves (inset). Right: the sliced preparation on the vibratome. (C) Illustration of the semi-intact preparation pinned (red dots) on the Sylgard-coated chamber. Population output is recorded in the vagus nerve (blue) while a vagal motoneuron is recorded by patch clamp (red). (D) Fluorescence image (4× magnification) of the semi-intact preparation showing the glowing vagal motoneurons (ellipses). (E) Bright-field (left) and fluorescence (right) images (40× magnification) of a motoneuron recorded using patch clamp. Diagrams were created using BioRender (biorender.com).

gravity-fed system at a ∼2 ml min^{-1}. To ensure chemosensitivity in the semi-intact preparation, three cells were alternatively superfused with aCSF bubbled with 1.5% CO_2 and 98.5% O_2 and after initial recordings they were exposed to aCSF gassed with 5% CO_2 (pH 7.4; hypercapnic acidosis for frogs, Fig. S1). For both groups, first, the vagal nerve root was localized by 4× imaging and pulled into a borosilicate glass pipette suction electrode using a 10 ml syringe (Fig. 1C). This pipette was pulled using a P87 horizontal pipette puller (Sutter Instruments, Novato, CA, USA), the tip was broken, and it was fire polished, adjusting to the nerve size. Respiratory-related extracellular nerve activity was amplified (×1000) and filtered (low pass, 1000 Hz; high pass, 10 Hz) using an AM-Systems 1800 amplifier (Sequim, WA, USA). The signal was digitized using Axon Digidata 1550B (Molecular Devices, San Jose, CA, USA) and recorded simultaneously to the cell using pClamp 11 (Molecular Devices, San Jose, CA, USA).

Journal of Experimental Biology (2022) 225, jeb244079. doi:10.1242/jeb.244079

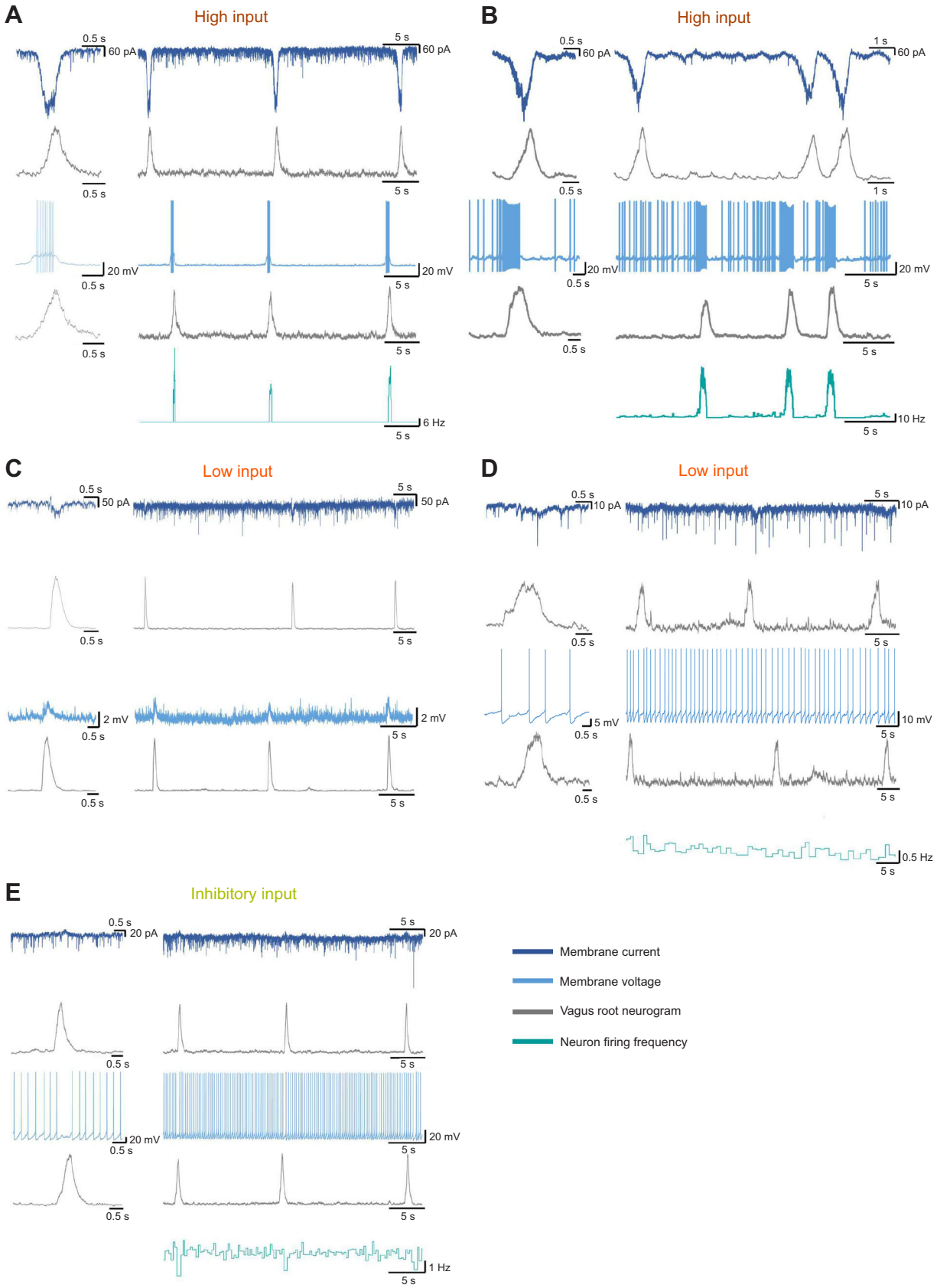

Fig. 2. Representative recordings of motoneurons in voltage-clamp and current-clamp mode in tandem with the extracellular motor output and cell firing frequency. (A) A motoneuron silent at rest receiving a high input RRSC and firing together with the lung burst. (B) A spontaneously firing neuron that increases firing frequency during high input RRSC. (C) Low input inward current leads to a small depolarization that does not evoke firing. (D) A neuron with low input that has a spontaneous firing pattern unchanged by RRSC. (E) A cell receiving an inhibitory input that causes an outward current in voltage-clamp mode and stops spontaneous firing in current-clamp mode.

Journal of Experimental Biology

Journal of Experimental Biology (2022) 225, jeb244079. doi:10.1242/jeb.244079

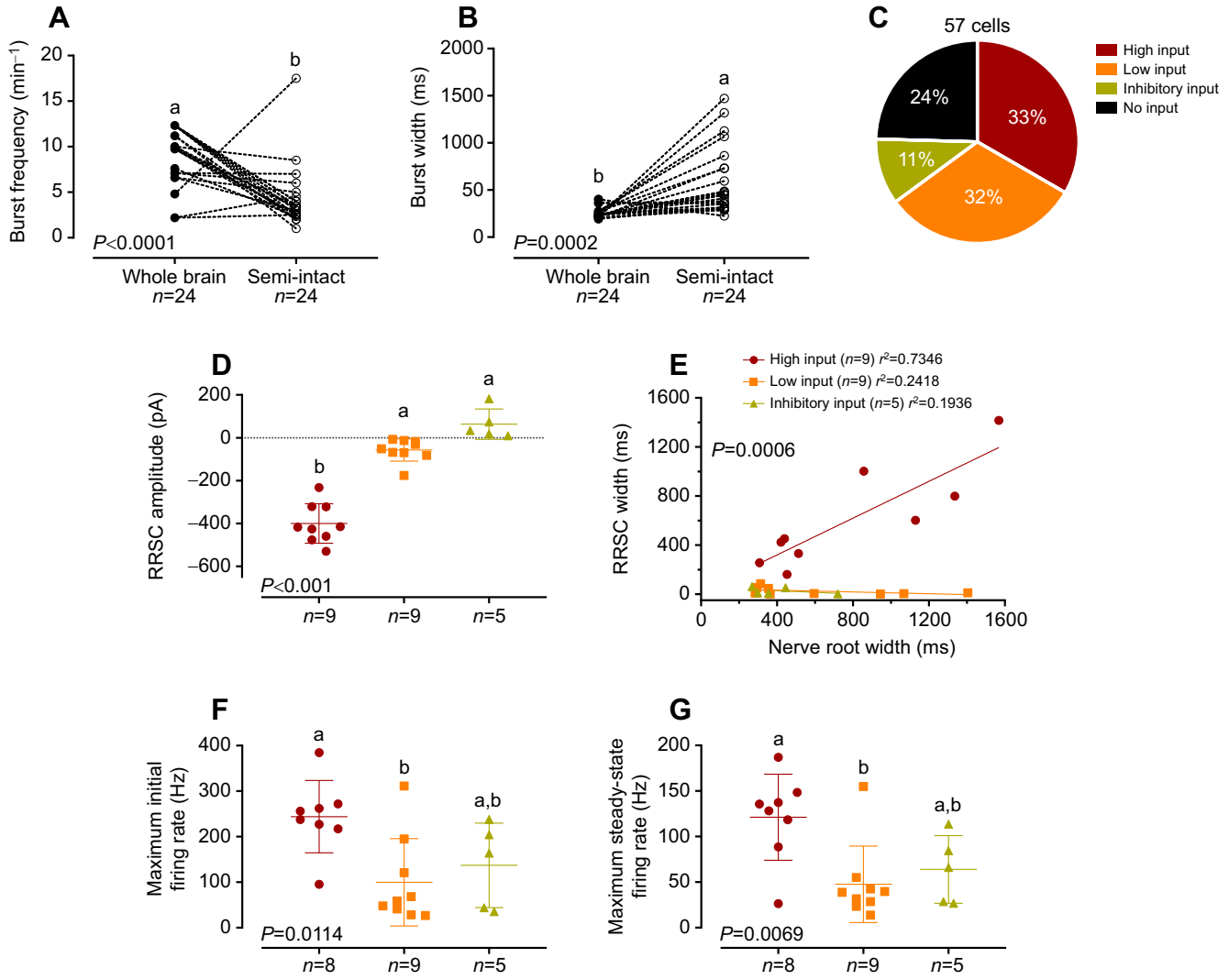

Fig. 3. Motor output, respiratory-related synaptic current (RRSC) and intrinsic properties of neurons receiving different inputs. (A) Frequency (B) and width of lung bursts recorded on the vagal root of the intact brainstem and the semi-intact preparation. (C) The number of cells found with each type of input. (D) Motoneurons receiving high input had a bigger RRSC amplitude than those receiving small input, while a positive amplitude was observed in inhibitory cells. (E) Width relationship between RRSC and motor output. Larger maximum initial (F) and steady-state (G) firing rates were observed in high input cells compared with low input cells. Different letters indicate differences among treatments; $P<0.05$ was considered statistically significant.

After obtaining a stable extracellular signal on the nerve root, regions containing labeled neurons were identified at 4× (Fig. 1D) and the cell bodies were located at 40× using fluorescence imaging (excitation, 540 nm: emission, 605 nm; Fig. 1E). Glass pipettes were pulled (P87 horizontal pipette puller, Sutter Instruments) with resistances between 2 and 4 MΩ when filled with a solution containing (in mmol l^{-1}): 110 potassium gluconate, 2 $MgCl_2$, 10 Hepes, 1 Na_2-ATP, 0.1 Na_2-GTP and 2.5 EGTA. Filled pipettes were attached to a head stage (CV203BU) connected to an MP-285 micromanipulator and an MPC-200 controller (Sutter Instruments). Gentle positive pressure was used to approach labeled neurons until a 'dimple' was observed in the bright field. At this moment, positive pressure was removed and the seal was formed (1 GΩ), applying gentle negative pressure by mouth. Whole-cell access was achieved by applying rapid negative pressure to rupture the gigaohm seal (Fig. 1E). Data were acquired in pClamp 11 software using an Axopatch 200B amplifier and Axon Digidata 1550B digitizer (Molecular Devices, San Jose, CA, USA).

Voltage and current protocols

We first recorded the cells in voltage-clamp mode to verify the respiratory-related synaptic currents (RRSCs) and spontaneous excitatory postsynaptic currents (sEPSCs) in neurons clamped at −66 mV. We then measured the membrane potential in current-clamp mode to determine the firing behavior of the neuron. Next, a step protocol was applied to determine input resistance and firing frequency–current (F–I) relationship (−150 to 1000 pA, 0.5 s steps). Extracellular activity was measured on the 4th branch of the vagus root concurrently to both voltage and current clamp. Identical ambient conditions were used for the whole-brain and semi-intact preparation (4 mmol l^{-1} K^+ aCSF bubbled with 1.5% CO_2 and 98.5% O_2).

Data analysis

Frequency and width of the extracellular fictive breaths were analyzed according to standard procedures (Bueschke et al., 2021a; Burton and Santin, 2020). Five minutes of extracellular burst frequency before slicing was compared with the frequency of the semi-intact preparation bursts averaging the activity recorded during

Journal of Experimental Biology (2022) 225, jeb244079. doi:10.1242/jeb.244079

both voltage- and current-clamp measurements. The non-respiratory bursts (very large) commonly observed in the root, which did not coincide in the signal observed in the cell, were not analyzed as we wished to focus on the activity of the respiratory network. The number of cells of each type (high, low, inhibitory and no respiratory-related synaptic input, Fig. 2 and see Results) was counted in all cells assessed in every frog utilized in the experiments regardless of the access quality. Only cells with low access resistance were used to measure voltage and current properties; thus, a smaller number of cells is displayed. Respiratory synaptic currents were evaluated in 1 min of recording in voltage-clamp mode, RRSC amplitude and width were analyzed using peak analysis of LabChart (ADInstruments Inc., Colorado Springs, CO, USA). Frequency and amplitude of the sEPSC were analyzed in bins of 5–10 s between the RRSCs totaling 30 s of gap-free recording. All events were inspected by eye to ensure the software detected sEPSCs and the analysis proceeded on LabChart 8 using the peak analysis function (ADInstruments Inc.). Events below 7.5 pA and with a rise time greater than 10 ms were not included in the analysis as their distinction from the noise is unreliable. Membrane potential was determined in between bursts with no current injection. Input resistance was calculated using Ohm's law ($R=\Delta V/\Delta I$) after recording the changes in voltage due to −100 pA current injection. In neurons that were silent at rest, rheobase was reported as the first current step that elicited an action potential. In cases where the neurons fired spontaneously, rheobase is reported as zero. Maximum firing rates are reported on a 1000 pA step or as the maximum firing rate before the cell entered depolarization block. The frequency rate of the two first spikes was described as the initial maximum firing, which was analyzed separately from the steady-state portion of the step (Zubov et al., 2021).

Analyzing the synaptic current, we observed cells receiving high, low, inhibitory and no respiratory-related synaptic input, which was visually distinguishable (see Results). Cells with no respiratory-related synaptic input had no discernible current in phase with the population burst on the vagus root. Cells receiving inhibitory input presented an outward current concurrently to the burst. A cell considered to receive low input always presented an inward RRSC smaller than 3 times the sEPSC value for that cell, and a cell considered to have high input always presented an inward RRSC amplitude at least 6 times larger than its sEPSC amplitude.

Statistical analysis

Raw data values from individual experiments accompanied by means±s.d. are shown for each variable. The burst frequency and width of the whole-brain and semi-intact preparation were compared using a paired *t*-test. The RRSC amplitude, width and cell properties of the different cell types were compared using one-way ANOVA. The slope of the linear regressions of amplitude between RRSC and population output were compared using ANCOVA. The differences among the averages were evaluated by Tukey's *post hoc* test. The number of preparations and cells in each type (n) are indicated in the figures. $P<0.05$ was considered statistically significant.

RESULTS AND DISCUSSION

The population burst frequency recorded from the vagal root of the semi-intact preparation was generally slower and wider than in the whole brain before slicing (Fig. 3A,B). However, this is still in the typical range of the intact brainstem preparation from juvenile and adult bullfrogs (Adams et al., 2021; Leclère et al., 2012; McLean et al., 1995). The increase in lung burst duration was similar to that observed in neonatal rats, where the rhythmic slice produced wider respiratory bursts compared with preparations preserving more of the medulla (Baertsch et al., 2019). Demonstrating the health state of the tissue, all semi-intact preparations produced consistent activity for >6 h in physiological K^+ and room temperature. Furthermore, the semi-intact preparation also exhibited CO_2/pH chemosensitivity, as well as episodic fictive breathing, and buccal oscillations, characteristic of intact preparations (Figs S1, S2).

In phase with the extracellular output, most vagal motoneurons presented an RRSC that often resulted in firing (Fig. 2). Using the semi-intact preparation, we observed four different types of neurons, described here as having high, low, inhibitory and no respiratory-related synaptic input. High input cells were characterized by a large inward RRSC recorded in voltage-clamp mode (−400±92 pA; Figs 2A-C and 3D) coinciding with every rising phase of the extracellular burst. The width of the RRSC spanned 73% of the lung motor output width (Fig. 3E). When monitoring these cells in current-clamp mode, the synaptic input evoked firing in cells that were silent at the baseline (Fig. 2A) and increased firing frequency of cells that were spontaneously firing (Fig. 2B). Low input cells showed a smaller inward RRSC (−57±51 pA; Figs 2C,D and 3D) in almost all respiratory bursts observed extracellularly. There was no correlation between the extracellular burst and RRSC width ($r^2=0.24$; Fig. 3E). In current-clamp mode, these smaller synaptic inputs did not bring silent neurons at baseline to the threshold (Fig. 2C) and did not change the firing rate of cells spontaneously firing (Fig. 2D). Inhibitory cells presented an outward RRSC (63±70 pA; Figs 2E and 3D) concurrent with every extracellular burst. Width was not correlated between extracellular/cellular input ($r^2=0.19$; Fig. 3E), but firing often stopped during the lung burst (Fig. 2E).

Motoneurons receiving high, low and inhibitory inputs were also analyzed for sEPSCs and intrinsic membrane properties in the period between respiratory bursts. When stimulating the neuron in current clamp, initial and steady-state maximum firing rates were larger in neurons with high input than in small input cells (59% and 60%, respectively), but no difference was found between those two types and neurons receiving inhibitory inputs (Fig. 3F,G). Spontaneous synaptic properties, rheobase, membrane potential and input resistance were not different among different cell types (Table 1).

Along the area containing labeled neurons, we found 33% with high input, 32% with low input, 11% with inhibitory input and 24% with no respiratory input (Fig. 3C). Given that our slicing procedure had a caudal bias, the most rostral cells in the pool may be under-represented here. Although we do not have an exact map of the cell types across the brainstem, we took note of the relative position of each cell. We found neurons with all types of

Table 1. Properties of the different cell types observed between RRSCs

	High input	Small input	Inhibitory input	*P*-value
sEPSC frequency (Hz)	11.66–5.96	7.66–4.34	5.63–3.15	0.0768
sEPSC amplitude (pA)	22.24–7.16	24.59–10.69	22.89–12.78	0.8724
Rheobase (pA)	187.50–152.95	200.00–321.13	70.00–75.83	0.5776
Membrane potential (mV)	–47.52–9.55	–55.365–9.67	–54.943–5.47	0.1507
Input resistance (MΩ)	74.33–26.39	200.48–180.09	196.76–135.36	0.1053

Data are means±s.d. RRSC, respiratory-related synaptic current; sEPSC, spontaneous excitatory postsynaptic current.

Journal of Experimental Biology (2022) 225, jeb244079. doi:10.1242/jeb.244079

respiratory-related synaptic input along the whole area studied; however, it was evident that high input motoneurons were more abundant in the caudal area aligned between the hypoglossal and vagal nerve roots. Small input neurons, in contrast, were more abundant in the rostral site closer to the vagus nerve root, and cells receiving inhibitory and no input were found scattered along with the motor pool.

Evaluation

Our work describes a new preparation that allows recording of labeled motoneurons within the respiratory network in adult bullfrogs. In this preparation, only the dorsal tissue covering the vagal motoneurons is sliced away, exposing them for whole-cell patch-clamp recording. Successful patch-clamp recordings showed respiratory-related synaptic currents and firing in tandem with the extracellular motor output, resembling the neuronal activity of the neonatal rat rhythmic slice (Koizumi et al., 2008). Even though slicing the dorsal brainstem may have caused some network damage, characterized by wider extracellular bursts with lower frequency compared with the intact brain, the semi-intact preparation had >6 h of consistent recordings in physiological K^+. This shows an advantage for studying motoneuron function, as rhythmic slices from rats rapidly change burst pattern and decrease frequency in physiological K^+, having only ∼108 min of longevity (Ruangkittisakul et al., 2006). Moreover, CO_2/pH chemosensitivity is preserved and preparations exhibited fictive breathing episodes (Figs S1, S2), as observed in the intact brainstem (Kinkead et al., 1994; Reid and Milsom, 1998).

Patch-clamp recordings revealed vagal motoneurons receiving high, low, inhibitory and no respiratory input. Synaptic excitation and inhibition observed here were similar to those of respiratory motoneurons of decerebrated frogs that also presented firing or hyperpolarization in phase with the lung burst (Kogo and Remmers, 1994). Optical imaging using a voltage-sensitive dye also shows motoneurons with firing stimulated or suppressed during lung bursts in the whole brain (Oku et al., 2008). Thus our semi-intact preparation recordings are comparable to recordings made *in vivo* and *in vitro* using the whole brainstem preparation, with the advantages of studying identifiable cells by labeling, using patch clamp, and in tandem with the axonal output.

The 4th branch of the vagus nerve contains axons that innervate the glottal dilator and potentially glottal constrictor muscles, which in most anurans are respectively responsible for opening the glottis after the air is enclosed in the oral cavity and may hold air in the lung following the buccal floor power stroke (Kogo et al., 1994; Sakakibara, 1984; West and Jones, 1975). Thus, the high input RRSC that generated firing in the laryngeal motoneurons contributes to the population burst observed on the vagal root, which likely dilates the glottis *in vivo* (Kogo and Remmers, 1994; Kogo et al., 1994). Motoneurons receiving low input here probably do not contribute to the fictive lung burst but may be recruited for glottal dilation in the case of an increase in respiratory drive. Similarly, the phrenic motor pool in rats is only partially activated in resting conditions, but respiratory challenges such as hypoxia recruit neurons that were not firing previously (Lee et al., 2009). Neurons with synaptic inhibition, in contrast, may keep the glottis closed during breath-hold periods, and stop firing during glottal dilation, as suggested by Kogo and Remmers (1994). Although the synaptic connections between respiratory rhythm generators and motor pools is still unknown, we speculate that the synaptic inputs observed here descend from the lung rhythm generator (Baghdadwala et al., 2015) via mechanisms analogous to those in mammals. For instance, in the neonatal rat slice, the pre-Bötzinger complex has excitatory and inhibitory interneurons that project to the hypoglossal premotor and motoneurons (Koizumi et al., 2013). Regarding cells with no input, they are also abundant in the phenic motor pool of mammals, being recruited for non-respiratory activities such as vomiting, coughing, sneezing and swallowing (Fogarty et al., 2018; Grelot et al., 1992; Hayashi and Fukuda, 1995; Lee and Fuller, 2011). Besides that, motoneurons with no respiratory-related input here could be also involved in calling as vocalization is regulated by motoneurons innervating the laryngeal muscles in frogs as well as breathing (Schmidt, 1965).

Interestingly, some intrinsic properties of the motoneurons were associated with the respiratory-related synaptic input, relating the neuron firing properties to its function in the network. Bullfrog vagal motoneurons are categorized in two types, slow and fast, based on their intrinsic membrane properties (Zubov et al., 2021). Here, high input neurons presented a higher maximum initial and steady-state firing rate compared with low input neurons. Those are the main characteristics distinguishing fast from slow vagal cells; thus, fast cells may constitute most of the high input neurons while slow cells may be the main type of cell receiving low input. Motoneurons receiving inhibitory input appear to be composed of both fast and slow types. Although maximum firing rate was related to the synaptic input, no differences across cell types existed in membrane potential, input resistance and rheobase (Table 1). This is not surprising as those properties are less influential in terms of classifying cell type (slow/fast), and intrinsic properties of the vagal motoneurons are highly variable (Zubov et al., 2021). Non-respiratory spontaneous synaptic properties were also not different among neurons receiving different inputs (Table 1).

Conclusion and perspectives

To advance the study of the cellular basis of breathing in non-mammalian models, we developed a semi-intact preparation that allows the recording of electrophysiological properties of motoneurons in the intact respiratory network. We expect this preparation to benefit the understanding of the respiratory network during the transition from gill to lung breathing and the acquisition of ischemia resistance following hibernation (Bueschke et al., 2021b; Janes et al., 2019b; Santin et al., 2017). Beyond that, this technique may be applied for different adult animals in multiple species with only a few adjustments, which may further contribute to understanding of the cellular basis of breathing across vertebrates. Additionally, as whole-cell patch clamp provides ready access to the cytoplasmic contents, single-cell molecular biology, such as RNA sequencing and real-time PCR, can be easily performed after patch clamp to connect cell physiology, network function and molecular mechanisms.

Acknowledgements

We thank Sarah Pellizzari for her input to build this preparation.

Competing interests

The authors declare no competing or financial interests.

Author contributions

Conceptualization: L.d.A.-S., J.M.S.; Methodology: L.d.A.-S.; Validation: L.d.A.-S.; Formal analysis: L.d.A.-S.; Investigation: L.d.A.-S.; Resources: J.M.S.; Data curation: L.d.A.-S.; Writing - original draft: L.d.A.-S.; Writing - review & editing: L.d.A.-S., J.M.S.; Visualization: L.d.A.-S., J.M.S.; Supervision: J.M.S.; Project administration: L.d.A.-S.; Funding acquisition: J.M.S.

Funding

This research was funded by grants from the U.S. Department of Defense (W911NF2010275) and the National Institutes of Health (1R01NS114514 and 1R15NS112920) to J.M.S. Deposited in PMC for release after 12 months.

References

Adams, S., Zubov, T., Bueschkle, N. and Santin, J. M. (2021). Neuromodulation or energy failure? Metabolic limitations silence network output in the hypoxic amphibian brainstem. *Am. J. Physiol.* **320**, 105-116.

Baertsch, N. A., Severs, L. J., Anderson, T. M. and Ramirez, J. M. (2019). A spatially dynamic network underlies the generation of inspiratory behaviors. *Proc. Natl. Acad. Sci. U. S. A.* **116**, 7493-7502. doi:10.1073/pnas.1900523116

Baghdadwala, M. I., Duchcherer, M., Paramonov, J. and Wilson, R. J. A. (2015). Three brainstem areas involved in respiratory rhythm generation in bullfrogs. *J. Physiol.* **593**, 2941-2954. doi:10.1113/JP270380

Bueschke, N., Amaral-Silva, L., Hu, M. and Santin, J. M. (2021a). Lactate ions induce synaptic plasticity to enhance output from the central respiratory network. *J. Physiol* **599**, 5485-5504. doi:10.1113/JP282062

Bueschke, N., Amaral-Silva, L. do, Adams, S. and Santin, J. M. (2021b). Transforming a neural circuit to function without oxygen and glucose delivery. *Curr. Biol.* **31**, R1564-R1565. doi:10.1016/j.cub.2021.11.003

Burggren, W. W. and Infantino, R. L. (1994). The respiratory transition from water to air breathing during amphibian metamorphosis. *Integr. Comp. Biol.* **34**, 238-246.

Burton, M. T. and Santin, J. M. (2020). A direct excitatory action of lactate ions in the central respiratory network of bullfrogs, *Lithobates catesbeianus*. *J. Exp. Biol.* **223**, jeb235705. doi:10.1242/jeb.235705

Fogarty, M. J., Mantilla, C. B. and Sieck, G. C. (2018). Breathing: Motor control of diaphragm muscle. *Physiology* **33**, 113-126. doi:10.1152/physiol.00002.2018

Fonseca, E. M., Noronha-de-Souza, C. R., Bícego, K. C., Branco, L. G. S. and Gargaglioni, L. H. (2021). 5-HT neurons of the medullary raphe contribute to respiratory control in toads. *Respir. Physiol. Neurobiol.* **293**, 103717. doi:10.1016/j.resp.2021.103717

Funk, G. D. and Greer, J. J. (2013). The rhythmic, transverse medullary slice preparation in respiratory neurobiology: Contributions and caveats. *Respir. Physiol. Neurobiol.* **186**, 236-253. doi:10.1016/j.resp.2013.01.011

Gargaglioni, L. H. and Milsom, W. K. (2007). Control of breathing in anuran amphibians. *Comp. Biochem. Physiol. A Mol. Integr. Physiol.* **147**, 665-684. doi:10.1016/j.cbpa.2006.06.040

Grelot, L., Milano, S., Portillo, F., Miller, A. D. and Bianchi, A. L. (1992). Membrane potential changes of phrenic motoneurons during fictive vomiting, coughing and swallowing in the decerebrate cat. *J. Neurophysiol.* **68**, 2110-20119. doi:10.1152/jn.1992.68.6.2110

Hayashi, F. and Fukuda, Y. (1995). Electrophysiological properties of phrenic motoneurons in adult rats. *Jpn. J. Physiol.* **45**, 69-83. doi:10.2170/jjphysiol.45.69

Hedrick, M. S. (2005). Development of respiratory rhythm generation in ectothermic vertebrates. *Respir. Physiol. Neurobiol.* **149**, 29-41. doi:10.1016/j.resp.2005.03.019

Janes, T. A., Fournier, S., Chamberland, S., Funk, G. D. and Kinkead, R. (2019a). Respiratory motoneuron properties during the transition from gill to lung breathing in the american bullfrog. *Am. J. Physiol. Regul. Integr. Comp. Physiol.* **316**, R281-R297. doi:10.1152/ajpregu.00303.2018

Janes, T., Rousseau, J. P., Fournier, S., Kiernan, E. A., Harris, M. B., Taylor, B. E. and Kinkead, R. (2019b). Development of central respirartory control in anurans: the role of neurochemicals in the emergence of air-breathing and the hypoxia response. *Respir. Physiol. Neurobiol.* **270**, 1-35. doi:10.1016/j.resp.2019.103266

Johnson, S. M., Wiegel, L. M. and Majewski, D. J. (2007). Are pacemaker properties required for respiratory rhythm generation in adult turtle brain stems *in vitro? Am. J. Physiol. Regul. Integr. Comp. Physiol.* **293**, R901-R910. doi:10.1152/ajpregu.00912.2006

Kinkead, R., Filmyer, W. G., Mitchell, G. S. and Milsom, W. K. (1994). Vagal input enhances responsiveness of respiratory discharge to central changes in pH/CO2 in bullfrogs. *J. Appl. Physiol.* **77**, 2048-2051. doi:10.1152/jappl.1994.77.4.2048

Kogo, N. and Remmers, J. E. (1994). Neural organization of the ventilatory activity in the frog, *Rana catesbeiana. II. J. Neurobiol.* **25**, 1080-1094. doi:10.1002/neu.480250905

Kogo, N., Perry, S. F. and Remmers, J. E. (1994). Neural organization of the ventilatory activity in the frog, *Rana catesbeiana*. I. *J. Neurobiol.* **25**, 1067-1079. doi:10.1002/neu.480250904

Koizumi, H., Wilson, C. G., Wong, S., Yamanishi, T., Koshiya, N. and Smith, J. C. (2008). Functional imaging, spatial reconstruction, and biophysical analysis of a respiratory motor circuit isolated *in vitro*. *J. Neurosci.* **28**, 2353-2365. doi:10.1523/JNEUROSCI.3553-07.2008

Koizumi, H., Koshiya, N., Chia, J. X., Cao, F., Nugent, J., Zhang, R. and Smith, J. C. (2013). Structural-functional properties of identified excitatory and inhibitory interneurons within pre-Bötzinger complex respiratory microcircuits. *J. Neurosci.* **33**, 2994-3009. doi:10.1523/JNEUROSCI.4427-12.2013

Kottick, A., Baghdadwala, M. I., Ferguson, E. V. and Wilson, R. J. A. (2013). Transmission of the respiratory rhythm to trigeminal and hypoglossal motor neurons in the American Bullfrog (*Lithobates catesbeiana*). *Respir. Physiol. Neurobiol.* **188**, 180-191. doi:10.1016/j.resp.2013.06.008

Lape, R. and Nistri, A. (2000). Current and voltage clamp studies of the spike medium afterhyperpolarization of hypoglossal motoneurons in a rat brain stem slice preparation. *J. Neurophysiol.* **83**, 2987-2995. doi:10.1152/jn.2000.83.5.2987

Leclère, R., Straus, C., Similowski, T., Bodineau, L. and Fiamma, M. N. (2012). Persistent lung oscillator response to CO2 after buccal oscillator inhibition in the adult frog. *Respir. Physiol. Neurobiol.* **183**, 166-169. doi:10.1016/j.resp.2012.06.030

Lee, K. and Fuller, D. D. (2011). Neural control of phrenic motoneuron discharge. *Respir. Physiol. Neurobiol.* **179**, 71-79. doi:10.1016/j.resp.2011.02.014

Lee, K. Z., Reier, P. J. and Fuller, D. D. (2009). Phrenic motoneuron discharge patterns during hypoxia-induced short-term potentiation in rats. *J. Neurophysiol.* **102**, 2184-2193. doi:10.1152/jn.00399.2009

Matesz, C. and Székely, G. (1996). Organization of the ambiguus nucleus in the frog (*Rana esculenta*). *Tongue Anatomy Kinemat. Dis.* **371**, 258-269.

McLean, H. A., Kimura, N., Kogo, N., Perry, S. F. and Remmers, J. E. (1995). Fictive respiratory rhythm in the isolated brainstem of frogs. *J. Comp. Physiol. A* **176**, 703-713. doi:10.1007/BF01021590

Oku, Y., Kimura, N., Masumiya, H. and Okada, Y. (2008). Spatiotemporal organization of frog respiratory neurons visualized on the ventral medullary surface. *Respir. Physiol. Neurobiol.* **161**, 281-290. doi:10.1016/j.resp.2008.03.002

Perry, S. F., Wilson, R. J. A., Straus, C., Harris, M. B. and Remmers, J. E. (2001). Which came first, the lung or the breath? *Comp. Biochem. Physiol. A Mol. Integr. Physiol.* **129**, 37-47. doi:10.1016/S1095-6433(01)00304-X

Reid, S. G. (2006). Chemoreceptor and pulmonary stretch receptor interactions within amphibian respiratory control systems. *Respir. Physiol. Neurobiol.* **154**, 153-164. doi:10.1016/j.resp.2006.01.016

Reid, S. G. and Milsom, W. K. (1998). Respiratory pattern formation in the isolated bullfrog (*Rana catesbeiana*) brainstem-spinal cord. *Respir. Physiol.* **114**, 239-255. doi:10.1016/S0034-5687(98)00091-7

Ruangkittisakul, A., Schwarzacher, S. W., Secchia, L., Poon, B. Y., Ma, Y., Funk, G. D. and Ballanyi, K. (2006). High sensitivity to neuromodulator-activated signaling pathways at physiological [K+] of confocally imaged respiratory center neurons in on-line-calibrated newborn rat brainstem slices. *J. Neurosci.* **26**, 11870-11880.

Sakakibara, Y. (1984). The pattern of respiratory nerve in the bullfrog. *Jpn. J. Physiol.* **34**, 269-282. doi:10.2170/jjphysiol.34.269

Santin, J. M. and Hartzler, L. K. (2016). Environmentally induced return to juvenile-like chemosensitivity in the respiratory control system of adult bullfrog, *Lithobates catesbeianus*. *J. Physiol.* **594**, 6349-6367. doi:10.1113/JP272777

Santin, J. M., Vallejo, M. and Hartzler, L. K. (2017). Synaptic up-scaling preserves motor circuit output after chronic, natural inactivity. *Elife* **6**, 1-18. doi:10.7554/eLife.30005

Schmidt, R. S. (1965). Larynx control and call production in frogs. *Copeia* **1965**, 143-147. doi:10.2307/1440715

Smith, J. C. and Feldman, J. L. (1987). In vitro brainstem-spinal cord preparations for study of motor systems for mammalian respiration and locomotion. *J. Neurosci. Methods* **21**, 321-333. doi:10.1016/0165-0270(87)90126-9

Vasilakos, K., Wilson, R. J. A., Kimura, N. and Remmers, J. E. (2005). Ancient gill and lung oscillators may generate the respiratory rhythm of frogs and rats. *J. Neurobiol.* **62**, 369-385. doi:10.1002/neu.20102

Vincen-Brown, M. A., Whitesitt, K. C., Quick, F. G. and Pilarski, J. Q. (2016). Studying respiratory rhythm generation in a developing bird: Hatching a new experimental model using the classic *in vitro* brainstem-spinal cord preparation. *Respir. Physiol. Neurobiol.* **224**, 62-70. doi:10.1016/j.resp.2015.08.007

West, N. H. and Jones, D. R. (1975). Breathing movements in the frog Rana pipiens. II. The power output and efficiency of breathing. *Can. J. Zool.* **53**, 345-353. doi:10.1139/z75-043

Wilson, R. J. A., Harris, M. B., Remmers, J. E. and Perry, S. F. (2000). Evolution of air-breathing and central CO2/H+ respiratory chemosensitivity: new insights from an old fish? *J. Exp. Biol.* **203**, 3505-3512. doi:10.1242/jeb.203.22.3505

Wilson, R. J. A., Vasilakos, K., Harris, M. B., Straus, C. and Remmers, J. E. (2002). Evidence that ventilatory rhythmogenesis in the frog involves two distinct neuronal oscillators. *J. Physiol.* **540**, 557-570. doi:10.1113/jphysiol.2001.013512

Zubov, T., Silika, S., Dukkipati, S. S., Hartzler, L. K. and Santin, J. M. (2021). Characterization of laryngeal motor neuron properties in the American bullfrog, *Lithobates catesbieanus*. *Respir. Physiol. Neurobiol.* **294**, 103745. doi:10.1016/j.resp.2021.103745

Zubov, T., Amaral-Silva, L. and Santin, J. (2022). Inactivity and Ca^{2+} signaling regulate synaptic compensation in motoneurons following hibernation in American bullfrogs. *bioRxiv*. https://doi.org/10.1101/2022.01.26.477843

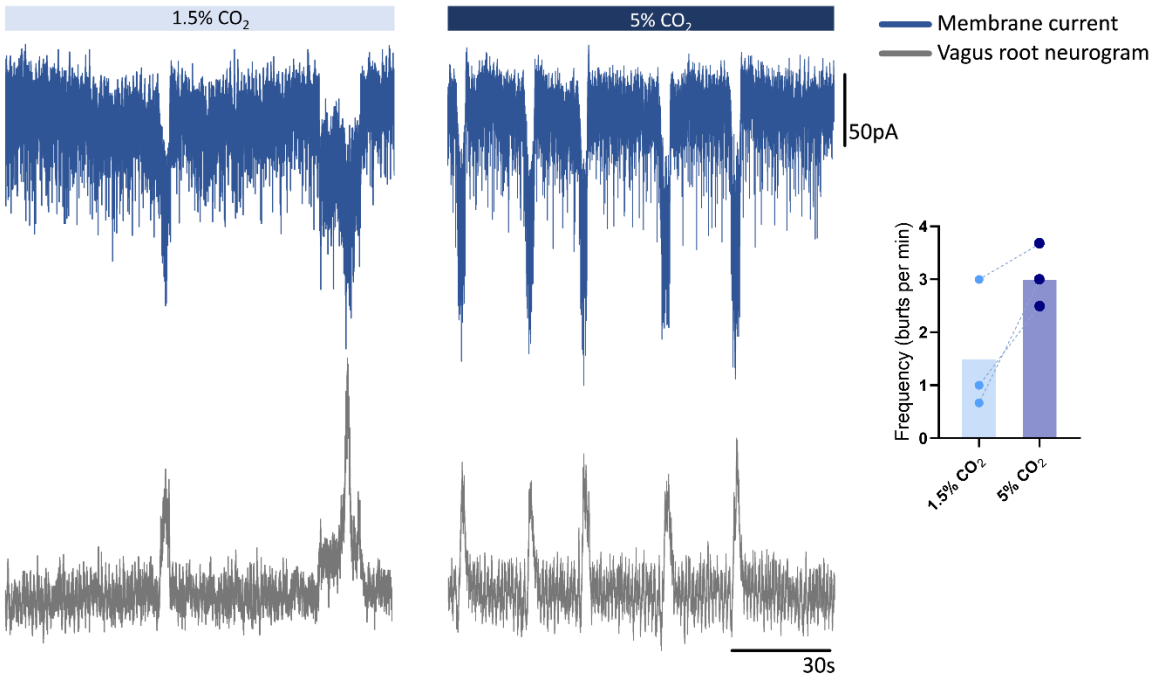

Fig. S1. Chemosensitivity is preserved in the semi-intact preparation. A) Representative traces showing increased burst frequency after 10 minutes of hypercapnia (aCSF CO_2 raised from 1.5% to 5%). B) All 3 preparations tested increased burst frequency in hypercapnia (average increase of 96%), which could be observed simultaneously in the cell respiratory synaptic input and in the population burst.

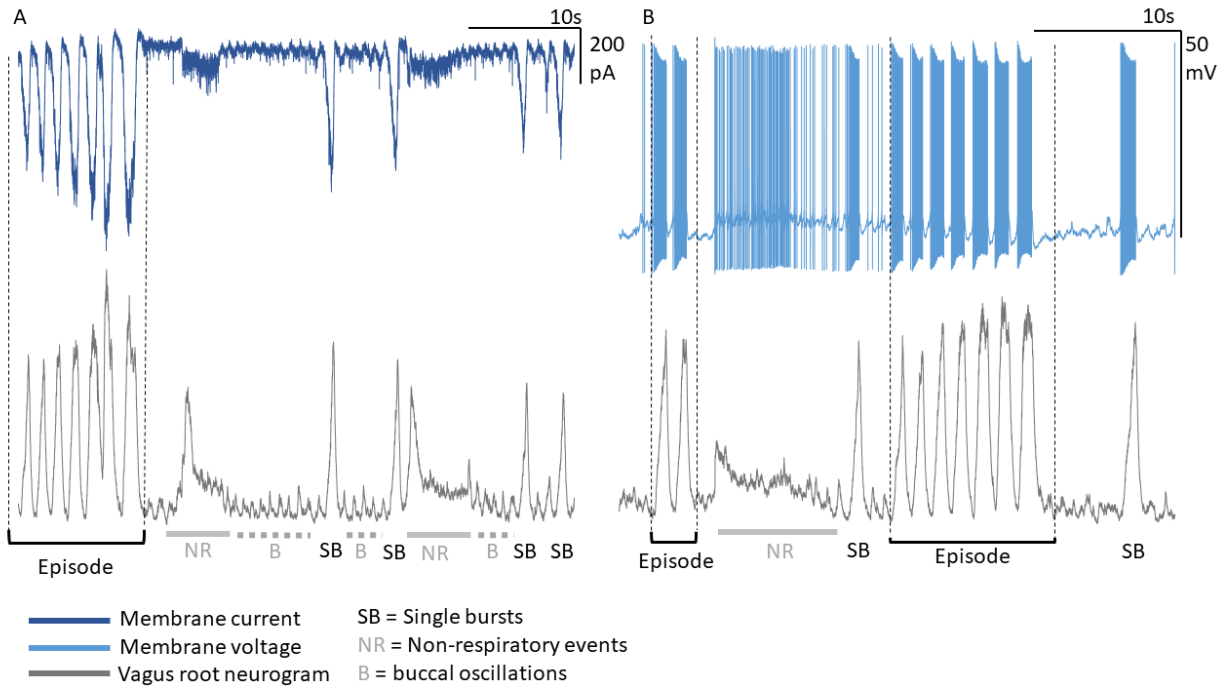

Fig. S2. The semi-intact preparation presents single and episodic bursts. Single bursts, doublets, episodic events, buccal oscillations, and non-respiratory events can be observed in the semi-intact preparation. Bursts occur concurrently with the respiratory-related synaptic current (A) and the motoneuron firing (B). The representative trace was recorded in control conditions (aCSF gassed with 1.5% CO_2 and 98.5% O_2).